# Ensemble measurement of the orientation-dependent variations in chromophore lifetimes near a dielectric interface

Andrea Pomozzi, Mi-Kyoung Park, and Maximilian Kreiter*
*Max Planck Institut für Polymerforschung, Ackermannweg 10, 55128 Mainz, Germany*
(Received 10 December 2008; revised manuscript received 13 March 2009; published 27 April 2009)

Excited-state lifetimes of fluorophores next to a dielectric interface depend on their orientation relative to the interface. We develop an experimental scheme to assess this effect quantitatively by recording fluorescence decay statistics of dye ensembles using polarized excitation and emission. These experiments allow for the determination of the relative orientation of excitation and emission dipole moments as well as the radiative and nonradiative decay rates of the chromphores. From the latter values, quantum yields can be deduced directly without using reference compounds.

DOI: 10.1103/PhysRevB.79.165435 PACS number(s): 32.50.+d, 78.68.+m

## I. INTRODUCTION

The radiative emission rate of a quantum emitter depends both on its transition dipole moment and on the dielectric environment. The latter defines the photonic mode density, corresponding to the phase space of possible emitted photons.[1,2] Emitters near a plane interface represent a particularly simple situation. On metal surfaces[3–6] the emission rate may change by orders of magnitude, partly corresponding to emitted photons and partly to dissipation in the metal. A nearby interface between two lossless dielectrics[7,8] has more moderate but still significant effects without introducing additional energy sinks.

Due to the broken symmetry of the system, the photonic mode density for emitting dipoles is strongly dependent on their orientation relative to the surface-normal vector.[9,10] This effect has been demonstrated experimentally using single-molecule techniques, first indirectly by correlating spectra and lifetimes[11] and later by directly measuring the dipole orientation and excited-state lifetime.[12]

A possible application of such lifetime changes was demonstrated by Brokmann *et al.*[13] They determined fluorescence quantum yields of individual semiconducting quantum dots via their lifetime change next to a dielectric interface. This approach is conceptually different from the classical method to determine fluorescence quantum yields by comparison to standard compounds[14] where the experimental uncertainty for the apparently simple problem of quantum yield determination is surprisingly high.[15] As a consequence, lifetime-related approaches have the potential to play an important role in the routine analysis of fluorescent species. In addition, lifetime variations near interfaces have been discussed as a possibility to increase the information content in fluorescence correlation spectroscopy.[16] Furthermore, they are of conceptual interest since they promise to shed some light on the effects of the molecular environment on the photonic mode density.[17,18]

The reported approaches to correlate the molecular orientation relative to an interface with their decay rate have been concentrated on single-molecule methods. They require specialized microscopic equipment and preparation techniques and well-trained and patient experimenters. At the same time they are restricted to extremely photostable molecules and suffer from biased selection of individuals.

Here, we outline and demonstrate an alternative ensemble method that allows correlation of molecular orientation and excited-state lifetime. We demonstrate the experimental feasibility using one model compound. With reasonable assumptions it is possible to directly obtain the fluorescence quantum yield and other photophysical parameters of this chromophore without additional adjustable parameters.

## II. EXPERIMENTAL DETAILS

Substrate preparation: UV-grade fused silica slides ($25\times25\times1$ mm$^3$) (PGO) were cleaned and activated for 45 min in a mixture of 10 ml $H_2O_2$ (34%), 10 ml $NH_3$ (32%), and 50 ml ultrapure water (Milli-Q). After rinsing with pure water they were vapor phase silanized in a closed vessel with 0.5 ml 3-aminopropyl-triethoxysilane (Sigma Aldrich Inc.) at 130 °C for 3 h. An extra rinsing step with water followed.

Dye functionalization: 24.5 mg poly(allylamine hydrochloride) (PAH) (Mw 15000, Sigma Aldrich) was dissolved in 5 ml bicarbonate buffer ($NaHCO_3$, 50 mM, pH=9). 50 $\mu$l of a DMF (N, N-dimethylformamide) solution of the chromophore FR636 (FR636 red reactive, Sigma Aldrich, 69296, concentration $5\times10^{-5}$ mol, $\lambda_{ex}=636$ nm, and $\lambda_{em}=665$ nm) was added while stirring. After 1 h in the dark, 200 ml acetone were added to precipitate the polymer. The precipitate was collected by filtering and dried.

Polyelectrolyte deposition: 0.0935 g (1 mmol repeat unit) of PAH was dissolved in 50 ml ultrapure water together with 10.29 g (10 mmol) of NaBr. 0.202 g (1 mmol repeat unit) of poly(styrene sulfonate) (PSS) (Mw 70000, Sigma Aldrich) was dissolved in 50 ml ultrapure water together with 4.049 g (32 mmol) of $MnCl_2$. Both solutions were filtered with syringe filter (pore size 0.2 nm) and brought to a pH=3 by addition of 0.5 ml HCl (0.1 N). The substrate was alternatively immersed in the solutions of PSS and PAH for 20 min each, with rinsing with water and drying between each deposition.

Fluorescence measurement: light pulses from a laser diode (Hamamatsu PLP10, $\lambda=634$ nm, pulse duration 110 ps, repetition rate 20 MHz) were coupled through a single-mode fiber. The light was collimated, passed a line filter and a linear polarizer, and was sent through a right-angle fused silica prism (Melles Griot, no. 01PQB002, $n=1.457\,02$ at

 

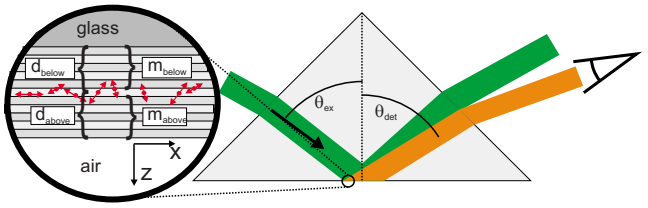


FIG. 1. (Color online) Sketch of the experimental geometry.

$\lambda = 632.8$ nm). The polyelectrolyte-coated slide was attached to its base by means of a low-fluorescent index oil (Nikon NF550, $n = 1.455$). The excitation light was impinging on the prism base under an angle of $\theta_{ex} = 0.72$ rad. Light emitted in the direction corresponding to $\theta_{det} = 0.85 \pm 0.03$ rad was detected by a photomultiplier (Becker & Hickl, PMC-100-20). Laser light was rejected by combined notch (Semrock) and long pass (Omega) filters. For each detected photon the arrival time since the experiment started (macrotime) as well as the time elapsed since the last excitation pulse (microtime) was recorded (Becker & Hickl, TCSPC-SPC630). The laser controller reference output was used for synchronization.

## III. EXPERIMENTAL CONCEPT

The experimental geometry is depicted in Fig. 1. A laser beam is impinging on the basis of a right-angled prism from the high-index (prism) side at an angle $\theta_{ex}$ relative to the surface normal. It excites chromophores which are deposited on the prism basis and the emitted fluorescence is detected; the detector position selects photons in a defined angular range $\theta_{det}$.

To place the chromophores at a defined distance from the interface between air and a dielectric with a higher refractive index, the polyelectrolytes poly(styrene sulfonate) and poly(allylamine) were used. They allow for the assembly of multilayers with a defined thickness at the nanometer scale.[19,20] One layer with covalently attached chromophores was embedded within a multilayer, with defined numbers of bilayers below ($m_{below}$) and above ($m_{above}$). This way, the dyes are placed at a defined $z$ position in a multilayer with adjustable distances $d_{below}$ and $d_{above}$ to the polymer-air interface and the polymer-glass interface, respectively.

### A. Single-molecule excitation

Let us now consider a chromophore which is described as a pair of excitation and emission dipole moments. Its excitation rate is given as the scalar product of exciting electrical field $\mathbf{E}$ and excitation dipole moment $\mathbf{p}_{ex}$,

$$\Gamma_{ex} \propto |\mathbf{p}_{ex} \cdot \mathbf{E}|. \quad (1)$$

At the dipole position, the local electrical field due to an incident plane wave is a superposition of the incident and reflected beam. Figures 2(a) and 2(b) show the absolute values of the three Cartesian field components assuming distances $d_{above} = 8.2$ nm, $d_{below} = 6$ nm, and a spacer refractive index $n_{PE} = 1.523$ normalized by the electrical field of the incident plane wave. Due to the similar refractive indices of the polymer and the glass, this situation is similar to the well-studied case[9,10] of dipoles at a defined distance from a single (air/glass) interface. These normalized fields or field transmission coefficients are calculated based on the transfer-matrix formalism.[21] Two linear polarizations are considered which are independent for plane layer systems, transverse magnetic ($p$) and transverse electric ($s$) polarization. For $p$ polarization two electrical field components $E_{px}$ and $E_{pz}$ exist which are, according to the coordinate system sketched in Fig. 1, parallel ($x$) and perpendicular ($z$) to the interface. Upon illumination at the critical angle, the field is almost purely $z$ polarized as it would be the case for $d_{above} = 0$ nm for a single interface. For $s$ polarization only a field component $E_{sy}$ parallel to the interface ($y$) exists. Figure 2(c) shows these fields for a fixed $\theta_{ex}$ as a function of the distance from the interface. Significant variations within the first 100 nm are seen.

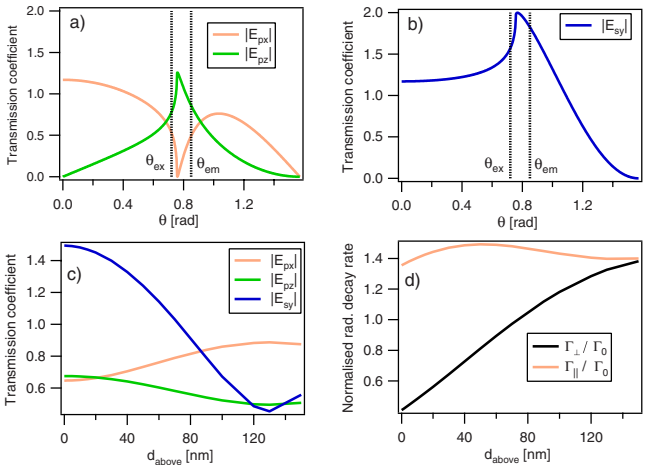


FIG. 2. (Color online) [(a) and (b)] Field transmission coefficients (local-field components normalized by the electrical field amplitude of the incident plane wave). The fields are evaluated for a three-layer system composed of fused silica ($n = 1.457$), polymer ($n = 1.523$), and air ($n = 1$). Furthermore, $d_{below} = 6$ nm and $d_{above} = 8.2$ nm are assumed. In (c) $\theta_{ex} = 0.687$ is set fixed and $d_{above}$ is varied. (d) Radiative decay rates as a function of $d_{above}$. Other parameters are identical.

### B. Single-molecule emission

For the emission process we consider a chromophore which has a radiative emission rate of $n\Gamma_0$ if embedded in a medium with refractive index $n$ in the absence of any interface. This formally corresponds to a radiative emission rate of $\Gamma_0$ in vacuum if apart from the different refractive index, all other influences of the nanoenvironment on the dye are unchanged. This is conceptually useful for the following analysis but we note that a real dye in vacuum will have a different radiative emission rate due to local-field effects.[22]

The excited-state lifetime of the chromophores close to an interface, or more generally any multilayered system, depends on the molecular orientation relative to the surface. As long as the emission process can be described by an emission dipole moment $\mathbf{p}_{em}$ which is fixed in space at an angle $\theta_{ed}$ with the surface-normal vector, we have

$$\Gamma_{\mathrm{em}} = \Gamma_{\mathrm{nr}} + \cos(\theta_{\mathrm{ed}})\Gamma_{\perp} + \sin(\theta_{\mathrm{ed}})\Gamma_{\parallel} = \Gamma_{\mathrm{rad}} + \Gamma_{\mathrm{nr}}. \quad (2)$$

$\Gamma_{\mathrm{nr}}$ is the nonradiative decay rate. The radiative rates for dipoles parallel and perpendicular to the interface, $\Gamma_{\parallel}$ and $\Gamma_{\perp}$, are depicted in Fig. 2(d) as a function of $d_{\mathrm{above}}$. The radiative decay rate for standing dipoles is significantly reduced close to the interface. With increasing distance from the air-polymer interface, similar decay rates are approached for both dipole orientations.

The probability that after excitation a photon is emitted in a certain solid angle covered by the detector with some polarization is

$$P = \frac{P(\Omega)}{P_{\mathrm{rad}}}\frac{P_{\mathrm{rad}}}{P_{\mathrm{rad}}+P_{\mathrm{nr}}} = \frac{\Gamma(\Omega)}{\Gamma_{\mathrm{rad}}+\Gamma_{\mathrm{nr}}}\frac{\frac{\Gamma(\Omega)}{\Gamma_0}}{\frac{\Gamma_{\mathrm{rad}}}{\Gamma_0}+\frac{\Gamma_{\mathrm{nr}}}{\Gamma_0}}. \quad (3)$$

Here, the ratios of probabilities $P$ and rates $\Gamma$ are equivalent. Normalization to the vacuum value $\Gamma_0$ facilitates the modeling. The emission rate and the directional distribution of the emitted radiation are obtained by considering the energy flux through a sphere around the emitter. For emission into some solid angle $\Omega$, integration over the corresponding sphere segment must be performed,

$$\frac{\Gamma(\Omega)}{\Gamma_0} = \frac{\int_{\Omega}\Phi(\mathbf{d})dA}{\int_{\mathrm{Sphere}}\Phi_0(\mathbf{d})dA}. \quad (4)$$

$\Phi$ and $\Phi_0$ denote the energy flux of dipoles in the presence of the multilayer system and in vacuum, respectively. The vector $\mathbf{d}$ connects the emitter and the sphere surface. For each point on the sphere we may consider two orthogonal linear polarizations of the electromagnetic field which are again labeled as $p$ and $s$ with electrical fields parallel to the unit vectors $\mathbf{e}_p$ and $\mathbf{e}_s$. They are defined relative to the plane of incidence containing the surface-normal vector and the "ray" connecting the emitter and the detector. Thus

$$\Phi(\vec{r}) = nc[|\mathbf{E}^p|^2 + |\mathbf{E}^s|^2], \quad (5)$$

where these fields are obtained for a dipole with emission dipole moment $\mathbf{p}_{\mathrm{em}}$,

$$\mathbf{E}^p = \mathbf{e}_p|\mathbf{p}_{\mathrm{em}}\cdot\mathbf{E}^p_{\mathrm{lc}}|k^2\frac{e^{i\mathbf{kd}}}{|\mathbf{d}|}\frac{1}{4\pi\varepsilon_0}, \quad (6)$$

and an equivalent expression for $s$ polarization. Here, we use the reciprocity theorem which connects emission of a dipole in a certain direction and local fields at the dipole position upon excitation from the same direction.[23,24] $\mathbf{E}^p_{\mathrm{lc}}$ denotes the local field that would be present at the dipole position if the system was illuminated by a plane wave of unit amplitude from the observation direction. For the multilayer system under study, $\mathbf{E}^p_{\mathrm{lc}}$ is directly connected to the field transmission coefficients shown in Fig. 2(a),

$$\mathbf{E}^p_{\mathrm{lc}} = \begin{pmatrix} E_{px} \\ 0 \\ E_{pz} \end{pmatrix}. \quad (7)$$

As a consequence, the $z$ and $x$ components of the molecules emission dipole moment determine the efficiency of the molecule to emit $p$-polarized light. At the critical angle $E_{px} \approx 0$, and therefore only the $z$ component contributes. So, a linear polarizer in front of the detector allows one to select radiation that comes predominantly from molecules with a dominating $z$ component for $p$ polarization. $s$-polarized emission stems predominantly from dipoles oriented along the $y$ axis.

### C. Modeling decay curves

Next we proceed to the analysis of the temporal distribution of photon emission relative to the excitation event. Assuming that a photon is emitted, the probability $P(\tau,\Delta\tau)$ that this emission event occurred within the time interval $[\tau, \tau+\Delta\tau]$ is

$$P(\tau,\tau+\Delta\tau) = \int_{\tau}^{\tau+\Delta\tau}\frac{dp}{d\tau'}d\tau', \quad (8)$$

with the emission probability density of an individual emitter,

$$\frac{dP}{d\tau} = [\Gamma_{\mathrm{rad}}+\Gamma_{\mathrm{nr}}]e^{-[\Gamma_{\mathrm{rad}}+\Gamma_{\mathrm{nr}}]\tau}. \quad (9)$$

In time-correlated single-photon counting experiments, the frequency of occurrence of photons with a certain time delay $\tau$ since the excitation event, the "microtime,"[25] is measured. In an ideal experiment the average number of detectable photons within a given experimental counting time $t_{\mathrm{exp}}$ (macrotime) which are within a given (micro) time interval $[\tau,\tau+\Delta\tau]$ since the last excitation, $N(\tau_{\mathrm{exp}},\tau,\Delta\tau)$, is obtained. This quantity can be modeled as

$$N(t_{\mathrm{exp}},\tau,\Delta\tau) = t_{\mathrm{exp}}\int_{\tau}^{\tau+\Delta\tau}F^{\mathrm{mol}}(\tau) \approx t_{\mathrm{exp}}F^{\mathrm{mol}}(\tau)\Delta\tau, \quad (10)$$

where $F^{\mathrm{mol}}$ is the product of the excitation rate [Eq. (1)], the detection probability [Eq. (3)], and the emission probability density [Eq. (9)] of an individual dye with a given position and orientation,

$$F^{\mathrm{mol}}(\tau) = \Gamma_{\mathrm{ex}}\frac{\Gamma(\Omega)}{\Gamma_{\mathrm{rad}}+\Gamma_{\mathrm{nr}}}[\Gamma_{\mathrm{rad}}+\Gamma_{\mathrm{nr}}]e^{-[\Gamma_{\mathrm{rad}}+\Gamma_{\mathrm{nr}}]\tau}$$
$$= \Gamma_{\mathrm{ex}}\frac{\Gamma(\Omega)}{\Gamma_0}\Gamma_0 e^{-\Gamma_0[(\Gamma_{\mathrm{rad}}/\Gamma_0)+(\Gamma_{\mathrm{nr}}/\Gamma_0)]\tau}. \quad (11)$$

$F^{\mathrm{mol}}$ has the dimension $s^{-2}$ and may be termed "rate density," pointing to its rate character in the macrotime and probability density character in the microtime domain. The superscript "mol" indicates that this equation applies to a single molecule. If many molecules are present, their individual contributions $F^{\mathrm{mol}}$, according to Eq. (11) must be added to an ensemble rate density,

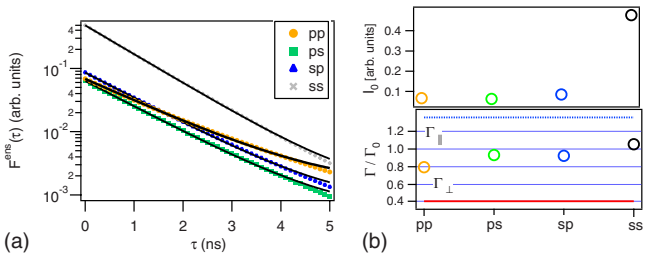


FIG. 3. (Color online) (a) Simulated decay curves for an ensemble of randomly oriented dyes. The lines are exponential fits. (b) Values for $I_{0,ed}$ and $\Gamma_{ed}/\Gamma_0$ as obtained by fitting.

$$F^{ens}(\tau) \sum_{mol} F^{mol}(\tau). \tag{12}$$

To calculate $F^{ens}(\tau)$, the orientation of $\mathbf{p}_{ex}$ and $\mathbf{p}_{em}$ must be specified for all molecules under study. While this probability distribution can be quite complex in general, for many relevant systems one may assume randomly oriented molecules. In this case one only has to specify the angle between $\mathbf{p}_{ex}$ and $\mathbf{p}_{em}$ to obtain a decay curve of the ensemble by summing a statistical ensemble of pairs $\mathbf{p}_{ex}$ and $\mathbf{p}_{em}$ with a fixed relative angle $\theta_{ex,em}$. It contains contributions from molecules with all possible orientation of the emission dipole relative to the interface, and in turn, different individual decay rates. Since two different linear polarizations, *p* and *s*, for both excitation and emission are considered, one may record four different decay curves. In Fig. 3 simulated decay curves assuming a $\Gamma_0=1$ s, random dye orientation and collinear absorption and emission dipole moments ($\theta_{ex,em}=0°$) are shown. The multilayer system is described by the parameters given in Fig. 2. The deviation from a monoexponential decay is not noticeable until the signal has decreased from its maximum value at $\tau=0$ by at least a factor of 10. In the experiment, this deviation cannot be resolved; therefore the information contained in such a decay curve may be condensed in the two parameters that are obtained by fitting: the signal strength $I_{0,ed}$ right after the exciting pulse and the apparent monoexponential decay rate $\Gamma_{ed}$ in the beginning. The subscripts *e* and *d* denote the excitation and detection polarizations which may both be either *p* or *s*. This yields a total of eight independent experimentally accessible quantities that can be used to characterize the chromophore under study. For the example discussed here, the resulting values for $\Gamma_{ed}$ and $I_{0,ed}$ are summarized in Fig. 3(b). For the *ss* configuration we obtain the highest intensity and an apparent decay rate that is close to the limiting case of a dye oriented parallel to the interface [dotted line in Fig. 3(b)]. For *pp* the intensity is significantly lower. $\Gamma_{pp}$ is approximately 1.3 times smaller than $\Gamma_{ss}$ but significantly larger than the value expected for dipoles purely oriented in the *z* direction. Intermediate apparent decay rates are found for *ps* and *sp* conditions. In the following, we are going to demonstrate that based on the four "decay curves" (*ss*, *ps*, *sp*, and *pp*), it is possible to determine the three intrinsic molecular parameters, $\Gamma_0$, $\Gamma_{nr}$, and $\theta_{em,ex}$ in a unique and reliable fashion.

## IV. MODEL SYSTEM AND DATA COLLECTED

The chromophore fluorescent red reactive 636 (FR636) was investigated. It was covalently attached to the polyelectrolyte poly(allylamine) (Mw 15000). The stoichiometry of the reactants corresponded to one chromophore per 5000 monomer units. A clean fused silica glass was functionalized by 3-aminopropyl-triethoxysilane and served as the support for the deposition of alternating poly(allylamine) and poly(styrene sulfonate) layers. First, 2.5 bilayers, starting with PSS were deposited, followed by the dye loaded PAH. Then, this layer was covered by additional bilayers of dye-free polyelectrolyte. Distances $d_{above}$ between the dye and the polymer-air interface between 8 and 80 nm were achieved with coverage between 2 and 10 additional polyelectrolyte bilayers. Illumination was provided by a *ps* laser diode ($\theta_{ex}=0.687$ with respect to the normal to the prism base) and the fluorescence photons emitted in $\theta_{em}=-0.884$ with respect to the normal to the prism base were recorded by a time-correlated single-photon counting card (Becker & Hickl, TCSPC-SPC630), recording for each photon the time elapsed since the excitation pulse (microtime $\tau$). Microtime histograms, normalized by total counting time $t_{exp}$ and excitation intensity $I_{ex}$ for one sample, are shown in Fig. 4. They equal the rate density in Eq. (11) up to a prefactor $\alpha$,

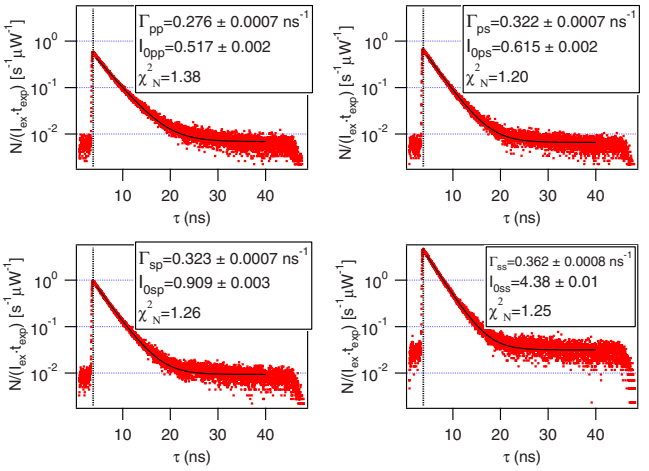


FIG. 4. (Color online) Microtime histograms. Counts per microtime interval are normalized by excitation intensity and total counting time. The time corresponding to the excitation pulse is indicated as dotted line. For the further evaluation, this time is taken as 0.

$$F^{ens} = \alpha \frac{N}{I_{ex} t_{exp}}. \tag{13}$$

The curves are well described by single exponential decays. The values determined for $I_0$ and $\Gamma_{ed}$ from each fit are displayed in the inset. We observe experimentally similar trends as predicted for the idealized model (Fig. 3); $\Gamma_{pp}$ is significantly smaller than $\Gamma_{ss}$ and $I_{0,pp}$ is significantly smaller than $I_{0,ss}$.

## V. DETERMINATION OF PHOTOPHYSICAL PARAMETERS

### A. Determine $\theta_{em,ec}$ and $I_0$

Next, we proceed with the quantification of molecular photophysical parameters. First, we note that optical trans-

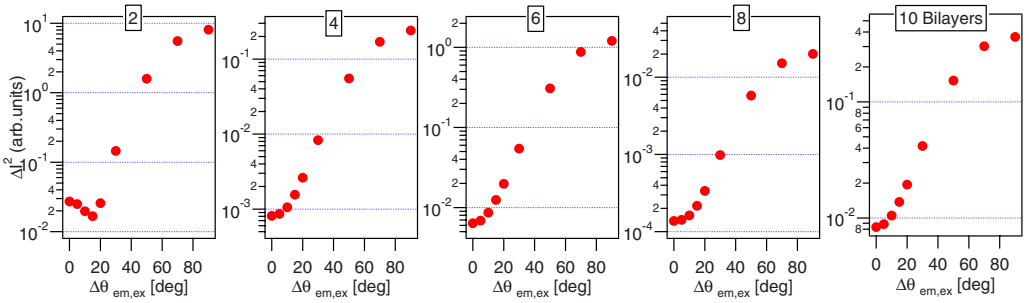


FIG. 5. (Color online) Sum-of-squares difference between calculated and experimental $I_0$ as a function of $\theta_{\mathrm{em,ex}}$. The number of bilayers is indicated on top of each graph. For the calculation, $d_{\mathrm{below}}=6$ nm and $d_{\mathrm{above}}=8.2/27.1/40.5/61.2/79.2$ nm were assumed.

mission characteristics of the setup, dye concentration, and detector quantum yield are experimental parameters that only lead to variations in the factor $\alpha$ in Eq. (13). Since these setup-related parameters are very difficult to quantify, we choose not to attempt a quantitative model of $\alpha$ and leave it as a free fitting parameter. Then, the only parameters that may be varied to model the experimental decay curves are $\Gamma_0$, $\Gamma_{\mathrm{nr}}$, and $\theta_{\mathrm{em,ex}}$. In principle, one could use a least-squares minimization routine to identify a set of $(\alpha,\Gamma_0,\Gamma_{\mathrm{nr}},\theta_{\mathrm{em,ex}})$ that represents the best fit to the experimental data. This approach is prohibitive due to the computational efforts required to generate one synthetic data set similar to the one shown in Fig. 3 with a given set of intrinsic parameters. Here, we present an alternative method to reach the same result.

We first consider $I_0$, the counts at $t=0$ which, from [Eq. (12)] is given assuming detection of all emitted photons

$$I_0 = t_{\mathrm{exp}}\Delta\tau F^{\mathrm{ens}}(\tau=0) = t_{\mathrm{exp}}\Delta\tau\sum_{\mathrm{mol}}\Gamma_{\mathrm{ex}}\frac{\Gamma(\Omega)}{\Gamma_0}\Gamma_0$$

$$= t_{\mathrm{exp}}\Delta\tau\Gamma_0\sum_{\mathrm{mol}}\Gamma_{\mathrm{ex}}\frac{\Gamma(\Omega)}{\Gamma_0}, \tag{14}$$

with the total counting time $t_{\mathrm{exp}}$ and the bin width $\Delta\tau$. Again neglecting all constant prefactors, this expression only depends on $\theta_{\mathrm{em,ex}}$. Therefore, $\theta_{\mathrm{em,ex}}$ can be determined from the four experimental $I_{0,\mathrm{ed}}$ $(e,d=p,s)$ by identifying the pair $(\alpha,\theta_{\mathrm{em,ex}})$ such that

$$\Delta I(\theta_{\mathrm{em,ex}},\alpha) = \sum_{p,s}(I^e_{0,\mathrm{ed}} - \alpha I^m_{0,\mathrm{ed}})^2 \tag{15}$$

is minimized. The superscripts $e$ and $m$ denote experimental and modeled quantities. For a fixed $\theta_{\mathrm{em,ex}}$ the optimum value for $\alpha$ is obtained analytically as

$$\alpha_{\mathrm{opt}} = \frac{\sum_{p,s} I^e_{0,\mathrm{ed}}\cdot I^m_{0,\mathrm{ed}}}{\sum_{p,s}(I^m_{0,\mathrm{ed}})^2}, \tag{16}$$

such that only the quantity

$$\Delta I^2(\theta_{\mathrm{em,ex}}) = \sum_{p,s}(I^e_{0,\mathrm{ed}} - \alpha_{\mathrm{opt}} I^m_{0,\mathrm{ed}})^2 \tag{17}$$

has to be minimized to retrieve $\theta_{\mathrm{em,ex}}$. Figure 5 shows $\Delta I^2(\theta_{\mathrm{em,ex}})$ for dye ensembles covered with polymer layers of different thickness. The values for $d_{\mathrm{below}}$ and $d_{\mathrm{above}}$ were determined by measuring polyelectrolyte multilayer thicknesses independently by ellipsometry (NANOFILM EP3) and with a profilometer (TENCOR P-10 Surface Profiler-KLA Tencor), average values are given in the caption of Fig. 5. For dyes covered by 4 bilayers and more, a consistent minimum for $\theta_{\mathrm{em,ex}}=0°$ is found, indicating that excitation and emission dipole moments are collinear. This is expected since we excite the chromophore close to its emission wavelength. Therefore the same electronic transition is responsible for excitation and emission. Furthermore, it suggests that the dyes are well immobilized such that their orientation does not change between excitation and emission. Chromophores only covered by a small amount of polymer show a slight deviation from this ideal behavior. Probably, a coating with 2 bilayers is too thin to be regarded as a bulk dielectric, and additional effects on very small length scales play a role here.

Figure 6(a) shows the measured $I_0$ values for the chromophores at different distances $d_{\mathrm{above}}$ from the polymer-air interface. Significant changes in the absolute intensities are obvious which are due to variations in the chromophore concentration. Figure 6(b) shows the same data normalized in comparison to the theoretical prediction assuming $\theta_{\mathrm{em,ex}}=0°$ and random dipole orientation. A remarkably good agreement of theory and experiment is found, given the difficulties of quantitative intensity measurements. Not only the $I_{0,ss}$ that is much higher than all other values but also the decrease in this difference with increasing coating thickness is nicely reproduced. The decrease in $I_{0,sp}$ and increase in $I_{0,ps}$ and $I_{0,ss}$ are seen as well. We conclude that randomly

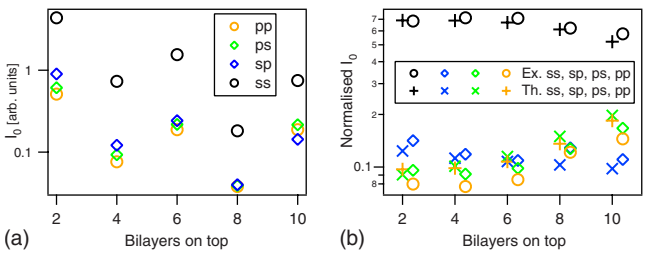


FIG. 6. (Color online) (a) $I_0$ as obtained from the fitting the decay curves. (b) Comparison between experimental and theoretical $I_0$. For comparison, both data sets were normalized such that $I_{0,pp}+I_{0,ps}+I_{0,sp}+I_{0,ss}=1$.

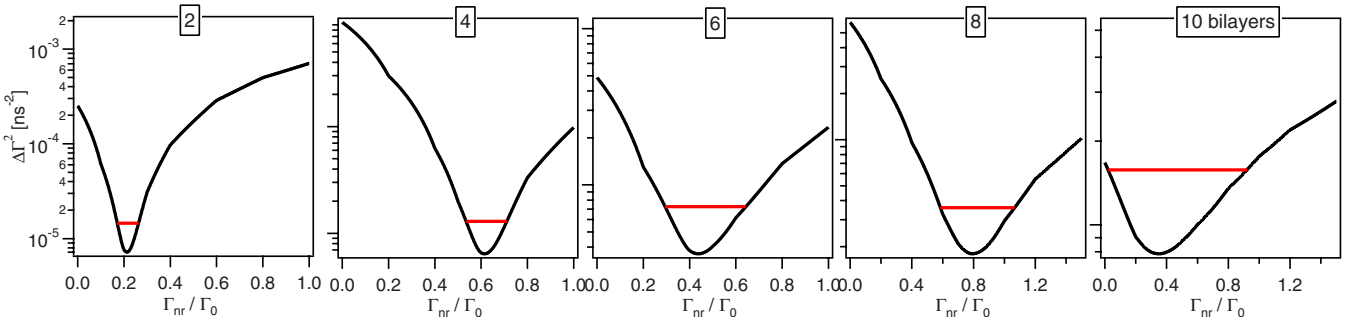


FIG. 7. (Color online) $\Delta\Gamma^2$ as a function of $\Gamma_{nr}/\Gamma_0$ for chromophores under polymer layers with different thickness.

oriented pairs of dipoles with $\theta_{em,ex}=0°$ are an appropriate description of our experimental situation. We will use these values for the further discussion. We furthermore note that significant deviations from this situation such as chromophores with a preferred orientation or large $\theta_{em,ex}$ would be readily seen in this analysis.

### B. Determine $\Gamma_0$ and $\Gamma_{nr}$

For the determination of the two remaining unknowns, $\Gamma_{nr}$ and $\Gamma_0$, we proceed in a way that is very similar to the determination of $\theta_{em,ex}$. We first note that $\Gamma(\Omega)/\Gamma_0$ and $\Gamma_{rad}=\Gamma_0$ do not depend on the actual value of $\Gamma_0$ but are intrinsic to the optical system. To make this clear, we introduce two normalized ($N$) parameters: $\Gamma(\Omega)^N=\Gamma(\Omega)/\Gamma_0$ and $\Gamma^N_{rad}=\Gamma_{rad}/\Gamma_0$. Similarly we introduce $\Gamma^N_{nr}=\Gamma_{nr}/\Gamma_0$ as a normalized molecular parameter that does not depend on $\Gamma_0$. With these abbreviations, Eq. (11) reads

$$F^{mol}(\tau)=\Gamma_{ex}\Gamma^N(\Omega)\Gamma_0 e^{-\Gamma_0[\Gamma^N_{rad}+\Gamma^N_{nr}]\tau}. \tag{18}$$

Since an overall scaling does not affect fitted apparent decay rates, we may alternatively consider for the ensemble response [Eq. (12)]

$$F^{ens'}(\tau)=\frac{F^{ens}(\tau)}{\Gamma_0}=\sum_{mol}\Gamma_{ex}\Gamma^N(\Omega)e^{-\Gamma_0[\Gamma^N_{rad}+\Gamma^N_{nr}]\tau}. \tag{19}$$

From this expression it is clear that again neglecting all prefactors, the only effect in $\Gamma_0$ is a scaling of the (micro) time axis. As a consequence, the ratio of the effective decay rates and the vacuum decay rate, $\Gamma^{ed}/\Gamma_0$, is constant. Then, we obtain a simple correspondence between modeled ($m$) and experimental ($e$) parameters as

$$\frac{\Gamma^m_{ed}}{\Gamma^m_0}=\frac{\Gamma^e_{ed}}{\Gamma^e_0}. \tag{20}$$

To identify the pair $(\Gamma_0,\Gamma_{nr}/\Gamma_0)$ that agrees best with the experiment, we have to minimize the difference $\Delta\Gamma$ between experimental and modeled decay constants,

$$\Delta\Gamma^2=\sum\left\{\Gamma^m_{ed}-\left[\frac{\Gamma^m_0}{\Gamma^e_0}\right]_{min}\Gamma^e_{ed}\right\}^2, \tag{21}$$

with

$$\left[\frac{\Gamma^m_0}{\Gamma^e_0}\right]_{min}=\frac{\sum_{ed}\Gamma^m_{ed}\cdot\Gamma^e_{ed}}{\sum_{ed}(\Gamma^e_{ed})^2}. \tag{22}$$

Figure 7 shows $\Delta\Gamma^2$ as a function of the remaining free parameter, $\Gamma_{nr}/\Gamma_0$. For dyes embedded below 4 polymer bilayers or more, a consistent minimum around $\Gamma_{nr}/\Gamma_0=0.5$ is seen. For chromophores covered with only 2 bilayers, again deviations from this simple model are obvious. From each of these curves, a $\Gamma_{nr}/\Gamma_0$ can be extracted as the position of minimum $\Delta\Gamma^2$. The error of $\Gamma_{nr}/\Gamma_0$ can be estimated from the points left and right of the minimum where $\Delta\Gamma^2$ has increased to twice its minimum value. This range is indicated by the horizontal lines in Fig. 7. This definition of the error is chosen since for a set of independent determinations of one quantity and assuming a Gaussian noise, the resulting interval would correspond to an error of one standard deviation ($\sigma$). We note that similar errors are obtained if the sample-to-sample variations in $I$ and $\Gamma$ are considered as statistical error while the error as obtained from the numerical fits of the decay curves are too small to explain these deviations from theory.

Simultaneously, the mean value and the standard deviation of $\Gamma^e_0/\Gamma^m_0$ is determined at the minimum and at the points of doubled $\Delta\Gamma^2$, respectively. Figures 8(a) and 8(b) show the values of these two parameters as determined from the five independent data sets. If we neglect the experiments where the dyes were very close to the surface, we obtain the weighted averages of $\Gamma_{nr}/\Gamma_0=0.59\pm0.07$ and $\Gamma_0=0.197\pm0.008$ ns$^{-1}$.

Figure 8(c) shows the experimentally obtained values for $\Gamma_{ed}$ together with the modeled values based on these weighted averages. Very good agreement is found for the decay rates. This indicates that first the simple model system described the experimental data quite well and that second by this ensemble experiment it is indeed possible to determine radiative and nonradiative decay rates with an acceptable accuracy.

## VI. APPLICABILITY FOR THE DETERMINATION OF LIFETIMES AND QUANTUM YIELDS

From the statistical analysis of our data, we obtain relative errors in $\Gamma_0$ and $\Gamma_{nr}/\Gamma_0$ of 4% and 11%, respectively, corresponding to a comparatively high accuracy for these quanti-

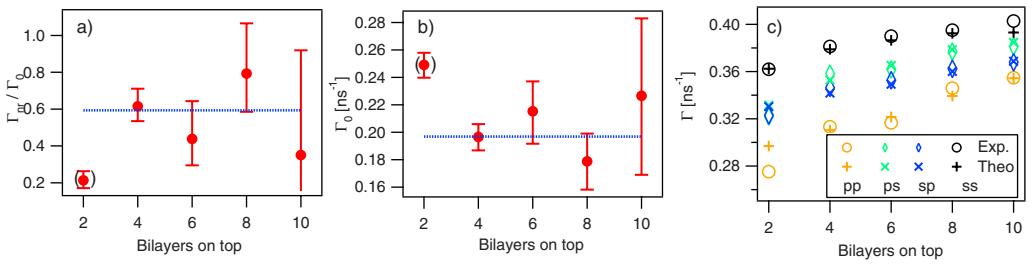


FIG. 8. (Color online) (a) Nonradiative and (b) radiative decay rates as obtained by the minimization. The horizontal line is the weighted average. (c) shows a comparison between modeled $\Gamma_{ed}$ and their experimental counterparts.

ties. Using the same physical effect and single-molecule methods, Brokmann *et al.*[13] arrived at a similarly accurate precision when determining the quantum yield of semiconducting quantum dots between 95% and 100%.

In spite of this apparently high accuracy, it is important to keep in mind that the analysis is based on several assumptions, which, although apparently well fulfilled for the model case studied here, must be checked again for a new system. One has to assure that the dye is indeed represented as a couple of excitation and emission dipole moments which are fixed in space and randomly oriented. The proper modeling of the surrounding media in terms of homogenous dielectric constants should be verified. Proper sample preparation avoiding chromophore aggregation is important as in any other quantum yield determination experiment.

We note furthermore that we obtain quantum yields for dyes embedded in a specific matrix. These values may differ significantly from the ones for dye solutions where quantum yields are usually measured. As a consequence, dyes should in general be characterized in the surrounding where they will be used for a certain application while comparison of values in different host media should be treated with care. One should point out furthermore that all methods to determine quantum yields are assuming chromophores which are identical and do not change in time. Blinking, for example, may lead to strong differences between the quantum yield measured via lifetime changes and using the classical method.[13] Dark but absorbing chromophores contribute to quantum yields measured by combined absorption and fluorescence emission spectroscopy but are not detected in the lifetime-based approaches. As a result, complementary information is obtained from the different approaches for such a more complex situation.

## VII. SUMMARY

In summary, we have developed a method to determine the angle between excitation and emission dipole moments as well as the radiative and the nonradiative decay rates of organic dyes. It is based on polarization-resolved excitation and detection of molecular fluorescence close to a dielectric interface, effectively using the different photonic mode densities for dipoles parallel and perpendicular to the interface. It has the conceptual advantage that it does not require calibration standards and can therefore be used in any host environment for quantum yield measurements. Therefore, we anticipate that such approaches for the determination of nonradiative decay rates will complement or even replace the "classical" method in the future.

## ACKNOWLEDGMENT

M.-K.P. acknowledges the Alexander von Humboldt Foundation.

*Corresponding author; kreiter@mpip-mainz.mpg.de

[1] W. L. Barnes, J. Mod. Opt. **45**, 661 (1998).
[2] E. M. Purcell, Phys. Rev. **69**, 681 (1946).
[3] B. C. Buchler, T. Kalkbrenner, C. Hettich, and V. Sandoghdar, Phys. Rev. Lett. **95**, 063003 (2005).
[4] R. R. Chance, A. Prock, and R. Silbey, Adv. Chem. Phys. **37**, 1 (1978).
[5] K. H. Drexhage, M. Fleck, H. Kuhn, F. P. Schäfer, and W. Sperling, Ber. Bunsenges. Phys. Chem. **70**, 1179 (1966).
[6] K. H. Drexhage, H. Kuhn, and F. P. Schäfer, Ber. Bunsenges. Phys. Chem **72**, 329 (1968).
[7] H. Khosravi and R. Loudon, Proc. R. Soc. London, Ser. A **433**, 337 (1991).
[8] K. H. Tews, O. Inacker, and H. Kuhn, Nature (London) **228**, 276 (1970).
[9] W. Lukosz and R. E. Kunz, J. Opt. Soc. Am. **67**, 1607 (1977).
[10] W. Lukosz and R. E. Kunz, J. Opt. Soc. Am. **67**, 1615 (1977).
[11] J. J. Macklin, J. K. Trautman, T. D. Harris, and L. E. Brus, Science **272**, 255 (1996).
[12] M. Kreiter, M. Prummer, B. Hecht, and U. P. Wild, J. Chem. Phys. **117**, 9430 (2002).
[13] X. Brokmann, L. Coolen, M. Dahan, and J. P. Hermier, Phys. Rev. Lett. **93**, 107403 (2004).
[14] D. F. Eaton, Pure Appl. Chem. **60**, 1107 (1988).
[15] S. Fery-Forgues and D. Lavabre, J. Chem. Educ. **76**, 1260 (1999).
[16] A. Benda, V. Fagul'ova, A. Deyneka, J. Enderlein, and M. Hof, Langmuir **22**, 9580 (2006).
[17] D. Toptygin, J. Fluoresc. **13**, 201 (2003).
[18] R. A. L. Vallee, N. Tomczak, L. Kuipers, G. J. Vancso, and N. F.

van Hulst,Phys. Rev. Lett. **91**, 038301 (2003).
[19] P. Bertrand, A. Jonas, A. Laschewsky, and R. Legras, Macromol. Rapid Commun. **21**, 319 (2000).
[20] G. Decher, J. D. Hong, and J. Schmitt, Thin Solid Films **210–211**, 831 (1992).
[21] P. Yeh, *Optical Waves in Layered Media* (Wiley, New York, 1998).
[22] F. J. P. Schuurmans, P. de Vries, and A. Lagendijk, Phys. Lett. A **264**, 472 (2000).
[23] L. Novotny and B. Hecht, *Principles of Nano-Optics* (Cambridge University Press, New York, 2006).
[24] M. Schmelzeisen, J. Austermann, and M. Kreiter, Opt. Express **16**, 17826 (2008).
[25] W. Becker, *The TCSPC Handbook* (Becker and Hickl, Berlin, 2006).